Available online at www.sciencedirect.com
ScienceDirect
Trans. Nonferrous Met. Soc. China 22(2012) 1620−1628
Transactions of Nonferrous Metals Society of China
www.tnmsc.cn

Fabrication and photocatalytic properties of Cu_2S/T-ZnO_w heterostructures via simple polyol process

WU De-zhi, FAN Xi-mei, TIAN Ke, DAI Jia, LIU Hua-rong

Key Laboratory of Advanced Technologies of Materials of Ministry of Education,
School of Materials Science and Engineering, Southwest Jiaotong University, Chengdu 610031, China

Received 23 September 2011; accepted 5 January 2012

Abstract: The Cu_2S/tetrapod-like ZnO whisker (T-ZnO_w) heterostructures were successfully synthesized via a simple polyol process employing the poly(vinyl pyrrolidone) (PVP) as a surfactant. The as-prepared heterostructures were characterized by X-ray diffraction (XRD), field emission scanning electron microscopy (FESEM), X-ray photoelectron spectroscopy (XPS) and Fourier transform infrared (FTIR). The photocatalytic properties of Cu_2S/T-ZnO_w nanocomposites synthesized with different PVP concentrations were evaluated by photodegradation of methyl orange (MO) under UV irradiation. The results show that the Cu_2S/T-ZnO_w nanocomposites exhibit remarkable improved photocatalytic property compared with the pure T-ZnO_w. The sample prepared with 3.0 g/L PVP shows an excellent photocatalytic property and the highest photodegradation rate of MO is 97% after UV irradiation for 120 min. Besides, the photocatalytic activity of the photocatalyst has no evident decrease even after four cycles, which demonstrates that the Cu_2S/T-ZnO_w photocatalyst exhibits an excellent photostability. Moreover, the photocatalytic mechanism of the Cu_2S/T-ZnO_w nanocomposites was also discussed.

Key words: Cu_2S/T-ZnO_w heterostructure; photocatalytic property; Cu_2S nanoparticle

1 Introduction

A great deal of efforts have been devoted in recent years to developing semiconductor photocatalysts with high photocatalytic activities for environmental protection purposes such as air purification, water disinfection, hazardous waste remediation, and water purification [1−4]. Among various semiconductor photocatalysts, ZnO has been recognized to be a preferable material for a variety of environmental applications, due to its high photosensitivity, non-toxic nature, low cost and chemical stability [5−7]. However, despite its great potential, the fast recombination of the photogenerated electron-hole pairs in the single phase ZnO leads to a very low photocatalytic efficiency and hinders the commercialization of this technology. Compared with single-phase photocatalysts, the heterostructures possess significant advantages for promoting the separation of electron-hole pairs and keeping reduction and oxidation reactions at two different reaction sites [8]. Recently, coupled semiconductors composed of ZnO and other metal oxides or sulfides have also been studied, such as combining ZnO with SnO_2, In_2O_3, CeO_2 and CdS semiconductor materials [9−13]. These results demonstrated that the nanocomposites fabricated by the coupling of different semiconductor materials will exhibit collective and enhanced property by mutual transfer of charge carriers (electrons and holes) from one semiconductor to another under irradiation and, consequently, achieving a higher photocatalytic activity [14−16].

Cu_2S is well known as a p-type semiconductor material with a narrow band gap (1.2 eV) [17]. It can be used in photosensitizer of various wide band-gap semiconductor photoanodes [18,19], electronic and optoelectronic chips [20−22], etc. The energy band structures of Cu_2S and ZnO are adequate to promote the electron transfer process where the photogenerated electrons can flow from Cu_2S to ZnO [23,24], and the charge carriers become physically separated upon generation. Therefore, the Cu_2S/tetrapod-like ZnO whisker (T-ZnO_w) composites were selected as a target

Foundation item: Project (2009AA03Z427) supported by the High-tech Research and Development Program of China; Project (2006z02-006-3) supported by the Science Foundation of Sichuan Province, China
Corresponding author: FAN Xi-mei; Tel: +86-28-87602714; Fax: +86-28-87600454; E-mail: fanximei@126.com
DOI: 10.1016/S1003-6326(11)61365-4

product to prepare for the photocatalytic degradation of organic pollutants.

It is widely acknowledged that organic surfactants, such as poly(vinyl pyrrolidone) PVP, have an important role in controlling the synthesis of nanomaterials, which determine not only the shape but also the size of the particles [25]. For example, LI et al [26] successfully synthesized Bi_2WO_6 by a hydrothermal process with the assistance of surfactant PVP. XU et al [27] prepared the size-controllable YVO_4:Eu^{3+} spheres by using PVP. SUN et al [28] successfully synthesized the silver nanowires employing PVP as the shape-direction agent. The studies showed that PVP played an important role in controlling the size of the nanomaterials.

The aim of this work is to investigate the role of Cu_2S in improving the photocatalytic property of ZnO. In this study, Cu_2S nanoparticles were grown on the surface of T-ZnO_w by a simple polyol process, in which PVP was used as a growth-directing agent. In order to achieve the aforementioned purpose, the effects of different PVP concentrations on the microstructure and photocatalytic property of the Cu_2S/T-ZnO_w nanocomposites were discussed.

2 Experimental

2.1 Sample synthesis

The T-ZnO_w was prepared by equilibrium gas controlling method using metallic zinc as the main raw material, which has been reported in our former research [29]. Cu_2S/T-ZnO_w nanocomposites were prepared by a simple polyol process in which T-ZnO_w, copper acetate (analytical grade), thiourea, diethylene glycol (DEG) and PVP were used. The fabrication process was as follows: firstly, 0.2 g of copper acetate was added into 80 mL of DEG with PVP concentrations of 0.6, 0.8, 1.0, 3.0 and 5.0 g/L, respectively and the solution was magnetically stirred for about 30 min; then, 2 g T-ZnO_w was poured into the obtained solutions; subsequently, 20 mL thiourea solution (0.005 mol/L) was slowly dropped into the above mixed solutions, respectively. Thereafter, the mixed suspension was maintained at 180 °C for 30 min. After the system was cool to room temperature naturally, the precipitates were collected after being washed with distilled water and ethanol three times, respectively, and then dried in a vacuum oven at 60 °C for 8 h. The Cu_2S/T-ZnO_w compound was obtained.

2.2 Sample characterization

The microstructure of the as-fabricated samples was investigated by X-ray diffraction (Panalytical X'pert PRO) with a Cu target and a monochronmator at 40 kV and 40 mA. Field emission scanning electron microscopy (FESEM, Fei Quanta 200, USA) with an accelerating voltage of 20 kV was conducted to analyze the morphologies of the photocatalysts. X-ray photoelectron spectroscopy (XPS) was performed with a PHI 5600 multitechnique system by a monochromatic Al K_α X-ray source. All core level spectra were referenced to the C 1s neutral carbon peak at 284.8 eV. FTIR spectra were recorded in the range from 450 to 4000 cm^{-1} using Fourier transform infrared spectrophotometer with KBr as the reference.

2.3 Photocatalytic property test

The photocatalytic properties of the samples were determined by measuring the photodegradation efficiency of MO aqueous solution. The photocatalytic degradation of MO was tested in our home-made instruments. Firstly, 50 mg of the photocatalysts prepared with different PVP concentrations were added into five beakers filled with 50 mL of MO aqueous solution (10 mg/L), respectively. Then, the obtained mixtures was stirred in dark for 20 min, and meanwhile irradiated by a UV-lamp (Hangzhou, China) with 254 nm emission wavelength at 25 °C. The solution was sampled every 20 min during UV irradiation in order to determine the degradation of MO, which was done by measuring the absorbance at 466 nm using a UV-Vis 2550 spectrophotometer. To further evaluate the photostability of the Cu_2S/T-ZnO_w, recycled experiments for the photodegradation of MO were also conducted.

3 Results and discussion

3.1 Structure and morphology

The X-ray diffraction patterns of pure T-ZnO_w, neat Cu_2S and Cu_2S/T-ZnO_w nanocomposites fabricated with different PVP concentrations were measured, respectively. As shown in Fig. 1, the diffraction peaks at 2θ=31.88°, 34.41°, 36.26°, 47.52° and 56.62° are

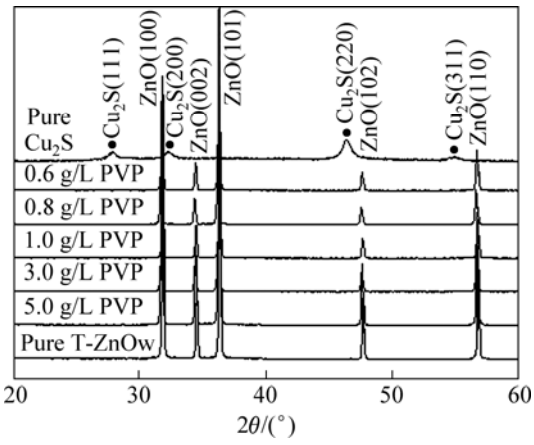

Fig. 1 XRD patterns of pure T-ZnO_w, neat Cu_2S and Cu_2S/T-ZnO_w nanocomposites prepared with PVP concentrations of 0.6, 0.8, 1.0, 3.0 and 5.0 g/L, respectively

ascribed to the typical wurtzite structure of ZnO (JCPDS card No. 36—1451). This indicates that the crystal structure of ZnO is intact during the fabrication process. The characteristic peaks at 2θ=27.86°, 32.29°, 46.31°, 54.82° correspond to the (111), (200), (220), (311) crystal planes of neat Cu_2S cubic phase (JCPDS card No. 84—1770). However, these diffraction peaks of Cu_2S are absence in the XRD patterns of Cu_2S/T-ZnO_w nanocomposites, which may be attributed to the very low amount of Cu_2S nanoparticles loaded on the surface of T-ZnO_w. This will be further discussed by the FESEM test and XPS analysis.

FESEM tests were carried out to observe the amount and morphology of Cu_2S in the Cu_2S/T-ZnO_w nanocomposites. Figure 2 shows the FESEM images of the pure T-ZnO_w and Cu_2S/T-ZnO_w nanocomposites

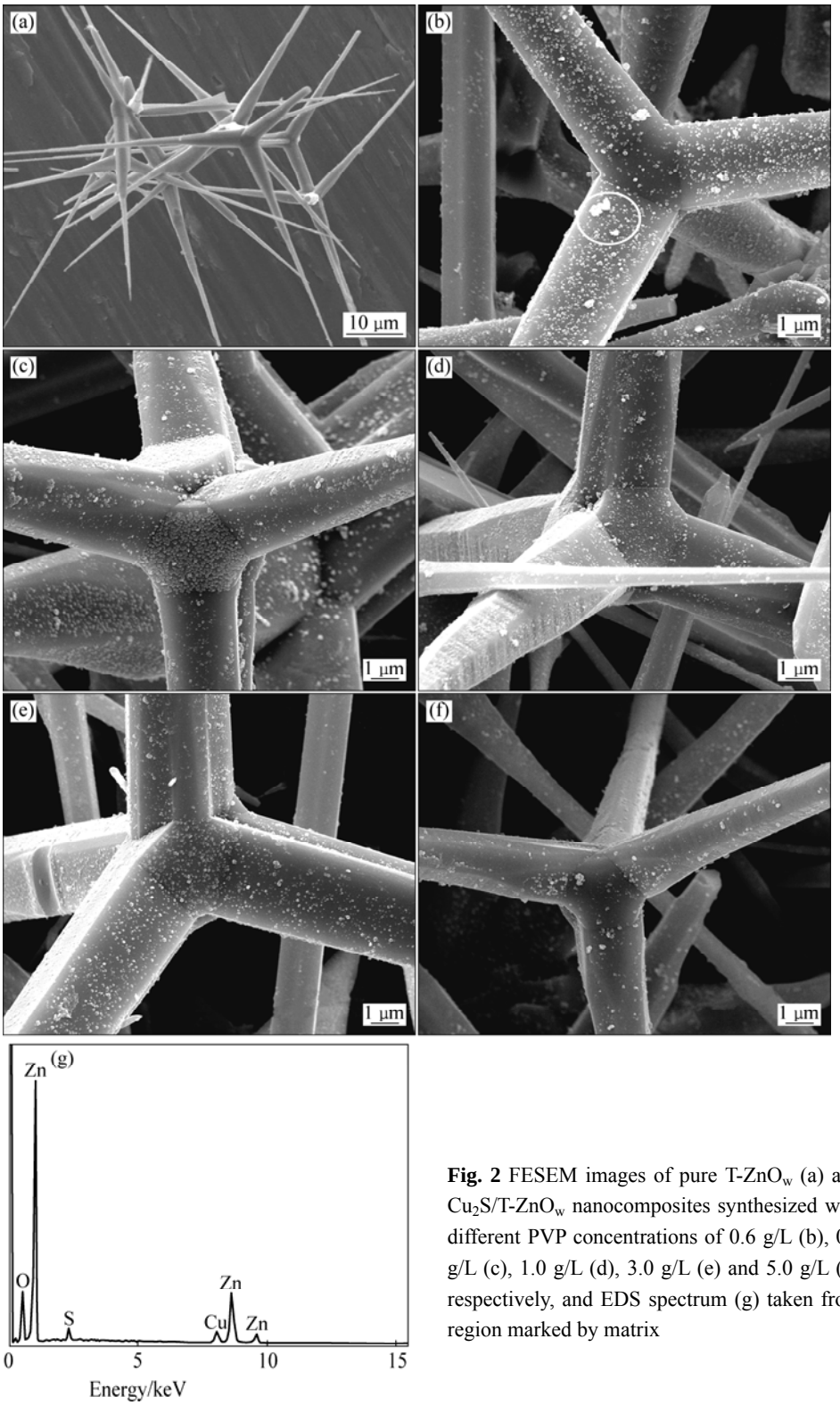

Fig. 2 FESEM images of pure T-ZnO_w (a) and Cu_2S/T-ZnO_w nanocomposites synthesized with different PVP concentrations of 0.6 g/L (b), 0.8 g/L (c), 1.0 g/L (d), 3.0 g/L (e) and 5.0 g/L (f), respectively, and EDS spectrum (g) taken from region marked by matrix

synthesized with the different PVP concentrations. Figure 2(a) gives the morphology of pure T-ZnO_w for a comparison. The length of the tetrapod arm of T-ZnO_w is 20−40 μm. Figures 2(b–f) show the morphologies of Cu_2S/T-ZnO_w nanocomposites with PVP concentrations of 0.6, 0.8, 1.0, 3.0 and 5.0 g/L, respectively. It was found that lots of nanoparticles were deposited on the surface of T-ZnO_w. When the concentration of PVP was relatively low, many nanoparticles and little agglomerates were obviously observed on the surface of T-ZnO_w. Besides, with the increase of PVP concentration from 0.8 to 3.0 g/L, the agglomerates gradually disappeared and the nanoparticles uniformly dispersed on the arms surface of T-ZnO_w. However, with further increasing the amount of PVP to 5.0 g/L, the nanoparticle amounts obviously decreased and many nanoparticles failed to deposit on the surface of T-ZnO_w (see Fig. 2(f)). The results can confirm that the appropriate amount of PVP is crucial to the synthesis of Cu_2S/T-ZnO_w nanomaterials. On one hand, an appropriate amount of PVP could efficiently prevent the aggregation of the nanoparticles and play an important role in obtaining monodispersed nanomaterials. On the other hand, when the excessive amount of PVP was used, the amount of Cu_2S nanoparticle on the surface of T-ZnO_w was reduced due to the strong absorption of PVP which hindered the deposition of Cu_2S nanoparticle on the surface of T-ZnO_w [24,25].

In order to reveal the chemical compositions of the nanoparticles, the area marked by a matrix in Fig. 2(b) was analyzed by the energy dispersive X-ray spectroscopy (EDS) and the result is shown in Fig. 2(g). It can be seen that the elements in the nanoparticles are Zn, O, Cu and S. These results suggest that the nanoparticles may be composed of Cu_2S and ZnO, and the surface chemical states will be further confirmed by XPS analysis. Moreover, the observed morphologies also indicate that the loading amount of Cu_2S nanoparticles is small, which matches the XRD results.

3.2 Surface chemical states and FTIR studies

The XPS spectra of Cu_2S/T-ZnO_w photocatalyst synthesized with 3.0 g/L PVP are shown in Fig. 3. All binding energy values in the XPS spectra were calibrated according to the information of C 1s (284.6 eV). From Fig. 3(a), Zn, O, Cu, S and C elements were observed and there are no peaks of other elements. The presence of C element mainly originated from the oil pump owing to vacuum treatment. Therefore, it was concluded that the Cu_2S/T-ZnO_w nanocomposites were composed of the

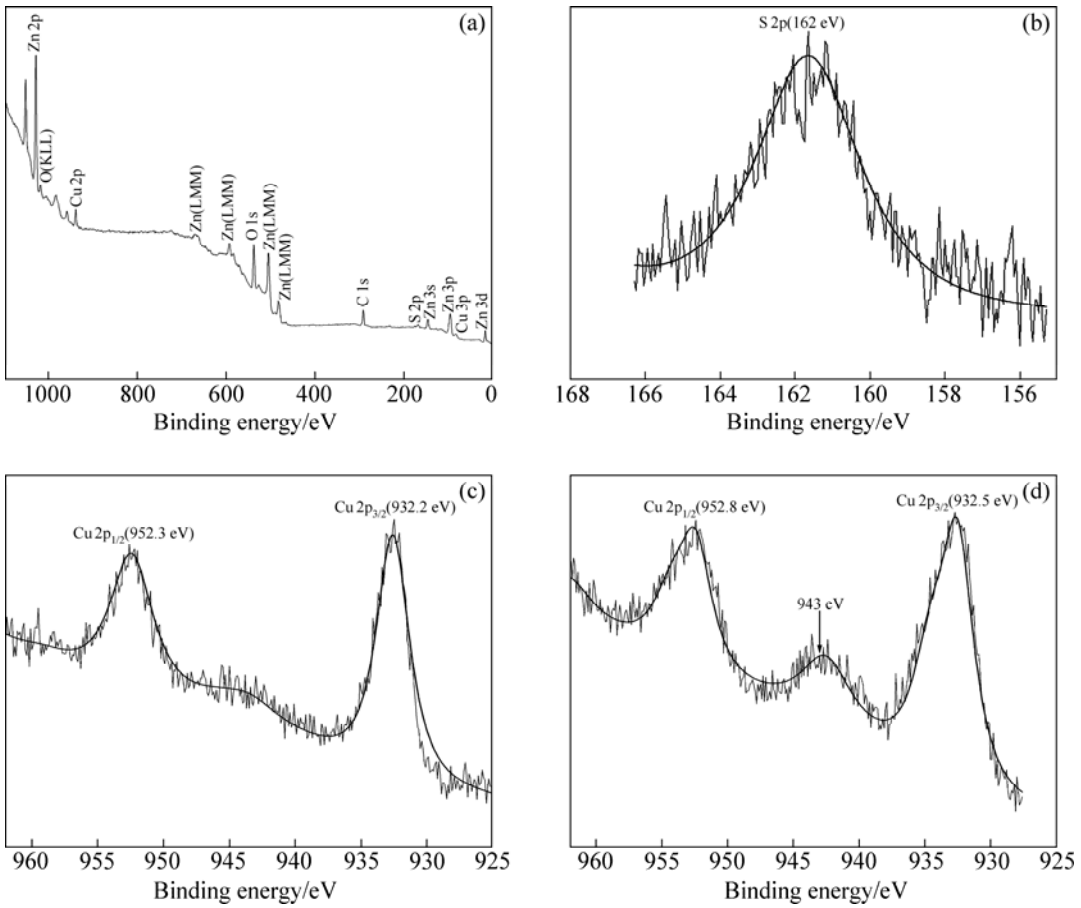

Fig. 3 XPS patterns of Cu_2S/T-ZnO_w nanocomposites prepared with 3.0 g/L PVP after the fourth recycled photocatalytic experiment: (a) Full spectrum; (b) Spectrum for S 2p; (c) Spectra for Cu $2p_{3/2}$ and Cu $2p_{1/2}$; (d) Spectra for Cu $2p_{3/2}$ and Cu $2p_{1/2}$

Zn, O, Cu and S elements. The binding energy of S 2p for Cu_2S/T-ZnO_w nanocomposites is 162 eV (Fig. 3(b)). The binding energy is smaller than that of sulfur and related compounds (S^0: 164.0 eV; chemisorbed SO_2: 163–165.5 eV; SO_3^{2-}: 166.4 eV; SO_4^{2-}: 168–170 eV), which is typical for S^{2-} ions [30]. The binding energy peaks of Cu $2p_{3/2}$ and Cu $2p_{1/2}$ for Cu_2S/T-ZnO_w nanocomposites locate at about 932.2 and 952.3 eV, respectively, and no "shake-up" peaks are found in the higher binding energy direction (Fig. 3(c)), which demonstrated that the copper in the nanocomposites was present in the +1 oxidation state (Cu^+) [31]. These results further confirmed that the nanoparticles on the surface of T-ZnO_w were composed of Cu_2S crystals, agreeing with the above-mentioned EDS results.

In order to further investigate the photostability of the Cu_2S/T-ZnO_w nanocomposites, XPS of the sample with 3.0 g/L PVP after the fourth recycled photocatalytic experiment is also presented in Fig. 3(d). It can be seen that there is a "shake-up" characteristic peak at about 943 eV associated with both Cu $2p_{3/2}$ and Cu $2p_{1/2}$ lines, which is generally assigned to the +2 oxidation state copper [31,32]. Therefore, the XPS results confirm the phase transformation from a little Cu_2S to CuS on the face of the Cu_2S/T-ZnO_w nanocomposites in MO solution after the fourth recycled UV light experiment.

Figure 4 shows the FTIR spectra of pure T-ZnO_w and Cu_2S/T-ZnO_w nanocomposites. The characteristic absorption peak at 504 cm^{-1} was assigned to Zn—O stretching vibration [33]. The absorption band at 3410 cm^{-1} corresponds to the stretching vibration of the hydroxyl, which came from the surface of pure ZnO particles. By comparison, the absorption peak at 1380 cm^{-1} was attributed to the stretching vibration of Cu—S in the Cu_2S/T-ZnO_w nanocomposites [34]. In addition, the hydroxyl stretching vibration in the Cu_2S/T-ZnO_w nanocomposites disappeared, which indicates that the Cu_2S nanoparticles were strongly bonded to the surface of T-ZnO_w. Besides, the characteristic peaks of the C=O, C—N and C—H groups from PVP did not appear in the FTIR spectrum, suggesting that the organic surfactant PVP had been removed completely from the Cu_2S/T-ZnO_w nanocomposites.

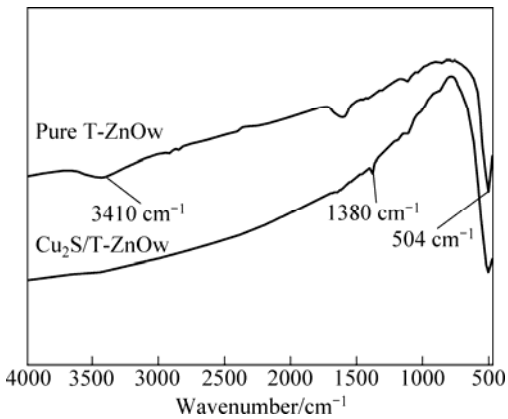

Fig. 4 FTIR spectra of pure T-ZnO_w and Cu_2S/T-ZnO_w nanocomposites prepared with 3.0 g/L PVP

3.3 UV-Vis diffuse reflectance spectroscopy

Figure 5 shows the UV-Vis diffuse reflectance spectra of T-ZnO_w and Cu_2S/T-ZnO_w photocatalysts. It can be seen that the optical absorption edges of the samples prepared with 0.6, 3.0 and 5.0 g/L PVP are shifted towards longer wavelength located at 393, 388 and 386 nm, respectively. Besides, the diffuse reflectance spectrum of the samples shows a long absorption band between 400 and 800 nm, while there is only a UV absorption edge located at about 381 nm for T-ZnO_w. The band gap energies (E_g) of the samples and T-ZnO_w were determined to be 3.15, 3.20, 3.21 and 3.25 eV, respectively, according to the following equation, E_g=1239.8/λ_g [35], where λ_g is the wavelength of the optical absorption edge which was obtained from the intersection of two tangents of the absorption curve.

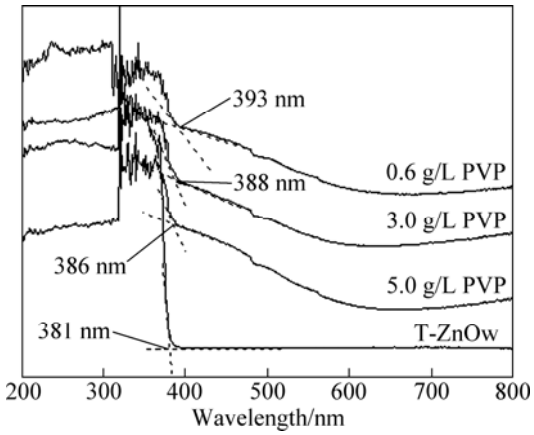

Fig. 5 UV-Vis diffuse reflectance spectra of T-ZnO_w and Cu_2S/T-ZnO_w photocatalysts prepared with 0.6, 3.0 and 5.0 g/L PVP, respectively

3.4 Photocatalytic property

Figure 6 shows the absorption curves of MO aqueous solution in the presence of Cu_2S/T-ZnO_w nanocomposites synthesized with 3.0 g/L PVP. Obviously, the absorbance peaks of MO aqueous solution weakened with the increase of the irradiation time, and the maximum absorbance peak located at 466 nm almost disappeared completely after UV irradiation for 120 min, due to the demethylation and hydroxylation of MO during the photocatalytic experiment [36].

The photocatalytic properties of Cu_2S/T-ZnO_w nanocomposites synthesized with different concentrations of PVP were evaluated in terms of the photodegradation efficiency of MO solution under UV light irradiation. In the present work, the degradation

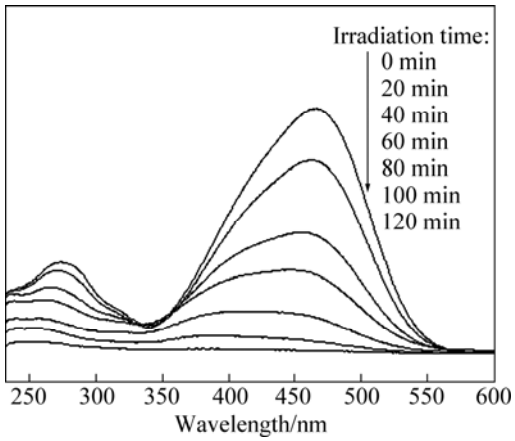

Fig. 6 Absorption curves of MO solution in the presence of Cu_2S/T-ZnO_w synthesized with 3.0 g/L PVP under different UV irradiation time

efficiency (R_d) is defined by the following equation [37]:

$$R_d = \frac{C_0 - C_t}{C_0} \times 100\%$$

where C_0 is the initial concentration of MO solution and C_t is the concentration of MO solution after the irradiation time of t. As shown in Fig. 7, the degradation efficiency of MO solution without any photocatalyst is less than 3% within 120 min under UV irradiation. In other words, the single UV irradiation has a minimal influence on the degradation of MO solution. For comparison, the photocatalytic experiment of neat T-ZnO_w was also introduced. The photodegradation efficiency of MO solution with the Cu_2S/T-ZnO_w nanocomposites is higher than that of the neat T-ZnO_w after UV irradiation for 120 min. The photocatalytic property of Cu_2S/T-ZnO_w nanocomposites increases with the increase of PVP concentration up to 3.0 g/L. However, with further increasing the PVP concentration

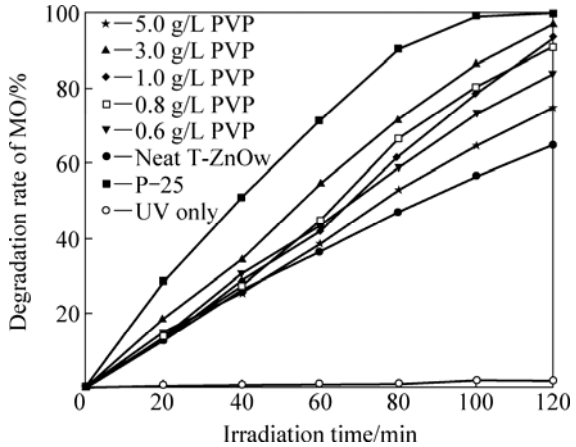

Fig. 7 Photodegradation curves of MO solution in the presence of Cu_2S/T-ZnO_w nanocomposites synthesized with different PVP concentrations

to 5.0 g/L, the degradation efficiency of MO solution declines obviously after irradiation for 120 min. Besides, the sample synthesized with 3.0 g/L PVP exhibits the highest photodegradation rate (97%) in photodegradation of MO for 120 min. In the photocatalytic experiments, the commercial TiO_2 (Degussa P−25) was used as the photocatalytic reference. It can be seen that the highest photodegradation rate of the sample almost reached that of P−25 after UV irradiation for 120 min in our home-made instruments.

The photoactivity enhancement for the coupled semiconductor/semiconductor heterostructure or metal/semiconductor heterostructure was attributed to the heterojuction existing in the composites, which might act as a rapid separation site for the photogenerated electrons and holes due to the difference in the energy level of their conduction bands and valence bands [38–41]. For the Cu_2S/T−ZnO_w heterostructure catalyst, the enhanced photoactivity was contributed to the many heterojuctions existing in the coupled Cu_2S/T-ZnO_w semiconductors. When increasing the PVP concentration, the Cu_2S nanoparticles uniformly dispersed on the surface of T-ZnO_w and thus increased the heterojuctions existing at the interface of Cu_2S and T-ZnO_w, which were beneficial to the photoactivity enhancement. However, when an excessive amount of PVP was used, the Cu_2S amount was reduced due to the strong absorption of PVP on the surface of T-ZnO_w, which resulted in reducing the amount of heterojuctions and thus reduced the photoactivity. Therefore, an appropriate PVP concentration was beneficial to enhancing the photoactivity of the Cu_2S/T-ZnO_w heterostructure catalysts.

The photostability of the Cu_2S/T-ZnO_w photocatalyst was also studied by cycled tests of the catalysts in fresh MO solution under UV light irradiation. Figure 8 shows the change of photodegradation efficiency from the first cycle to the fourth cycle using the sample with 3.0 g/L PVP. It can be seen that the degradation efficiency of the sample slightly drops after every cycle, which is mainly ascribed to the phase transformation of a little Cu_2S to CuS. This agrees well with the XPS results (Fig. 3(d)). However, the photodegradation efficiency of the sample even after the fourth cycle is still much higher than that of pure T-ZnO_w, which demonstrates that the Cu_2S/T-ZnO_w photocatalyst possesses an excellent photostability.

The enhanced activity of the coupled Cu_2S/T-ZnO_w nanocomposites under UV irradiation can be interpreted using a schematic diagram of the energy band structure of Cu_2S/T-ZnO_w heterojunction, as shown in Fig. 9. It is reported that interparticle transfer of charge carriers contributes to the enhanced photocatalytic efficiency of coupled semiconductors when the energies of valence and conduction bands properly match [42]. The

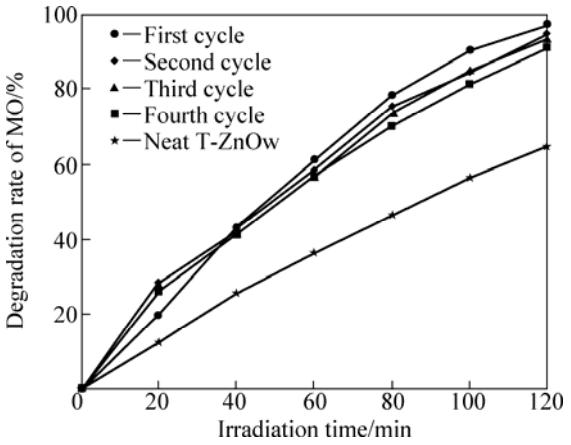

Fig. 8 Photodegradation curves of MO solution in the presence of Cu_2S/T-ZnO_w synthesized with 3.0 g/L PVP for different recycled experiments

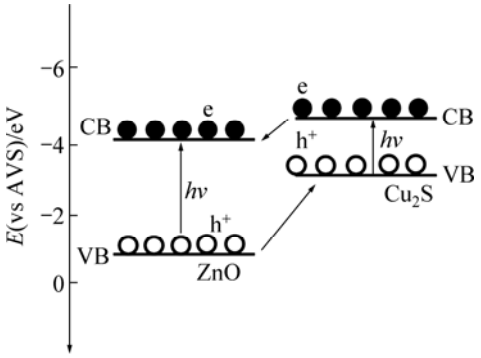

Fig. 9 Schematic representation of excitation and separation of electrons and holes for Cu_2S/T-ZnO_w heterostructure under UV irradiation

conduction band (CB) edge of Cu_2S (−4.44 eV vs absolute vacuum scale (AVS)) is higher compared with ZnO (−4.19 eV vs AVS); the valence band (VB) edges of Cu_2S and ZnO are located at −3.34 eV and −0.99 eV (vs AVS), respectively [24,43,44]. On the basis of the different positions of their band gaps, the photoexcited electrons can transfer from the conduction band of Cu_2S to that of ZnO, contrarily, the photoexcited holes immigrate from the valence band of ZnO to that of Cu_2S under UV irradiation. Besides, the interface between the Cu_2S/T-ZnO_w heterostructure might act as a rapid separation site for the photogenerated electrons and holes, which resulted in enhancing the separation efficiency of photogenerated electrons and holes, and thus enhanced the photocatalytic activity in the photocatalytic process [38,41,45,46]. The photocatalytic reactions were possibly proposed as follows:

$$Cu_2S/ZnO+h\nu \rightarrow Cu_2S(e+h^+)/ZnO(e+h^+) \rightarrow Cu_2S(h^+)/ZnO(e) \quad (1)$$

$$e+O_2 \rightarrow \bullet O_2^- \quad (2)$$

$$h^++OH^- \rightarrow \bullet OH \quad (3)$$

$$\bullet O_2^-+H_2O \rightarrow \bullet HO_2+OH^- \quad (4)$$

$$\bullet HO_2+H_2O \rightarrow \bullet H_2O_2+\bullet OH \quad (5)$$

$$H_2O_2 \rightarrow 2\bullet OH \quad (6)$$

$$\bullet OH+MO \rightarrow \text{Oxidation products} \quad (7)$$

Under UV light irradiation, the coupled semiconductor catalysts were excited to generate the electron (e)−hole (h^+) pairs. The photogenerated electrons emigrated to the surface of ZnO, and the photogenerated holes transferred to that of Cu_2S. Then the electrons reacted with the dissolved oxygen to yield the superoxide anion radical ($\bullet O_2^-$), which continuously participated in the photocatalytic reaction to generate the hydroperoxy ($\bullet HO_2$) and then generated the hydroxyl radical (•OH) which was responsible for the oxidation decomposition of methyl orange. Besides, the holes were trapped by the surface hydroxyl to produce the hydroxyl radical. Finally, the model pollutant (MO) was oxidized by the hydroxyl radical in the photocatalytic process [47]. Of course, the higher hydroxyl radical content was beneficial to enhancing the photoactivity of the Cu_2S/T-ZnO_w catalyst.

4 Conclusions

The Cu_2S/T-ZnO_w heterostructures were successfully synthesized by a simple polyol process. The heterostructure catalysts show much better photocatalytic activity and photostability in photodegradation of MO under UV light compared with the pure T-ZnO_w, and the Cu_2S/T-ZnO_w heterostructure catalyst with 3.0 g/L PVP content exhibits the optimal photocatalytic activity. In future, the coupled Cu_2S/T-ZnO_w nanocomposites may be a new photocatalyst to be utilized in environmental pollution control.

References

[1] HOFFMANN M R, MARTIN S T, CHOI W, BAHNEMANN D W. Environmental applications of semiconductor photocatalysis [J]. Chemical Reviews, 1995, 95: 69−96.

[2] HU C, YU J C, HAO Z, WONG P K. Photocatalytic degradation of triazine-containing azo dyes in aqueous TiO_2 suspensions [J]. Applied Catalysis B, 2003, 42: 47−55.

[3] YU Y, YU J C, YU J, KWOK Y C, DING L, GE W, CHE Y, ZHAO J, WONG P K. Enhancement of photocatalytic activity of mesoporous TiO_2 by using carbon nanotubes [J]. Applied Catalysis A, 2005, 289: 186−196.

[4] YU Y, YU J C, CHAN C Y, CHE Y, ZHAO J, DING L, GE W, WONG P K. Enhancement of adsorption and photocatalytic activity of TiO_2 by using carbon nanotubes for the treatment of azo dye [J]. Applied Catalysis B, 2005, 61: 1−11.

[5] SAKTHIVEL S, NEPPOLIAN B, SHANKAR M V, ARABINDOO B, PALANICHAMY M, MOORAGESAN V. Solar photocatalytic

degradation of azo dye: Comparison of photocatalytic efficiency of ZnO and TiO_2 [J]. Solar Energy Materials & Solar Cells, 2003, 77: 65−82.

[6] KHODJA A A, SEHILI T, PILICHOWSKI F, BOULE P. Photocatalytic degradation of 2-phenylphenol on TiO_2 and ZnO in aqueous suspensions [J]. Journal of Photochemstry and Photobiology A, 2001, 141: 231−239.

[7] GU C D, CHENG C, HUANG H Y, WONG T L, WANG N, ZHANG T Y. Growth and photocatalytic activity of dendrite-like ZnO@Ag heterostructure nanocrystals [J]. Crystal Growth & Design, 2009, 9: 3278−3285.

[8] YANG D, PARK S E, LEE J K, LEE S W. Sonochemical deposition of nanosized Au on titanium oxides with different surface coverage and their photocatalytic activity [J]. Journal of Crystal Growth, 2009, 311: 508−511.

[9] ZHENG L R, ZHENG Y H, CHEN C Q, ZHAN Y Y, LIN X Y, ZHENG Q, WEI K M, ZHU J F. Network structured SnO_2/ZnO heterojunction nanocatalyst with high photo catalytic activity [J]. Inorganic Chemistry, 2009, 48: 1819−1825.

[10] WANG Z Y, HUANG B B, DAI Y, QIN X Y, ZHANG X Y, WANG P, LIU H X, YU J X. Highly photocatalytic ZnO/In_2O_3 heteronanostructures synthesized by a coprecipitation method [J]. Journal of Physical Chemistry C, 2009, 113: 4612−4617.

[11] MA T Y, YUAN Z Y, CAO J L. Hydrangea-like meso-/macroporous ZnO−CeO_2 binary oxide materials: Synthesis, photocatalysis and CO oxidation [J]. European Journal of Inorganic Chemistry, 2010, 716−724.

[12] WU Y, TAMAKI T, VOLOTINEN T, BELOVA L, RAO K V. Enhanced photoresponse of inkjet-printed ZnO thin films capped with CdS nanoparticles [J]. The Journal of Physical Chemistry Letters, 2010, 1: 89−92.

[13] XU F, VOLKOV V, ZHU Y, BAI H Y, REA A, VALAPPIL N V, SU W, GAO X Y, KUSKOVSKY I L, MATSUI H. Long electron-hole separation of ZnO−CdS core-shell quantum dots [J]. Journal of Physical Chemistry C, 2009, 113: 19419−19423.

[14] ROLISON D R. Catalytic nanoarchitectures-the importance of nothing and the unimportance of periodicity [J]. Science, 2003, 299: 1698−1701.

[15] ARAI T, YANAGIDA M, KONISHI Y, IWASAKI Y, SUGIHARA H, SAYAMA K. Efficient complete oxidation of acetaldehyde into CO_2 over $CuBi_2O_4$/WO_3 composite photocatalyst under visible and UV light irradiation [J]. Journal of Physical Chemistry C, 2007, 111: 7574−7577.

[16] LI B X, WANG Y F. Facile synthesis and photocatalytic activity of ZnO−CuO nanocomposite [J]. Superlattices and Microstructures, 2010, 47: 615−623.

[17] GORAI S, GANGULI D, CHAUDHURI S. Synthesis of 1D Cu_2S with tailored morphology via single and mixed ionic surfactant templates [J]. Materials Chemistry and Physics, 2004, 88: 383−387.

[18] SAVELLI M, BOUGNOT T J. Problems of the Cu_2S/CdS cell [C]. New York: Springer-Verlag, 1979: 213−256.

[19] DACHRAOUI M, VEDEL J. Improvement of cuprous sulphide stoichiometry by electrochemical and chemical methods [J]. Solar Cells, 1987, 22: 187−194.

[20] PINTILIE I, PENTIA E, PINTILIE L, PETRE D, CONSTANTIN C, BOTILA T. Growth and characterization of PhS deposited on ferroelectric ceramics [J]. Journal of Applied Physics, 1995, 78: 1713−1718.

[21] INDREA E, BARBU A. Indirect photon interaction in PbS photodetectors [J]. Applied Surface Science, 1996, 106: 498−501.

[22] POP I, NASCU C, IONESCU V, INDREA E, BRATU I. Structural and optical properties of PbS thin films obtained by chemical deposition [J]. Thin Solid Films, 1997, 307: 240−244.

[23] PENG M, MA L L, ZHANG Y G, TAN M, WANG J B, YU Y. Controllable synthesis of self-assembled Cu_2S nanostructures through a template-free polyol process for the degradation of organic pollutant under visible light [J]. Materials Research Bulletin, 2009, 44: 1834−1841.

[24] XU Y, SCHOONEN M A A. The absolute energy positions of conduction and valence bands of selected semiconducting minerals [J]. American Mineralogist, 2000, 85: 543−556.

[25] YIN Y, ALIVISATOS A P. Colloidal nanocrystal synthesis and the organic-inorganic interface [J]. Nature, 2005, 437: 664−669.

[26] LI Y Y, LIUJ P, HUANG X T, LI G Y. Hydrothermal synthesis of Bi_2O_6 uniform hierarchical microsheres [J]. Crystal Growth & Design, 2007, 7: 1351−1355.

[27] XU W, WANG Y, BAI X, DONG B, SONG H W. Controllable and synthesis and size-dependent luminescent properties of YVO_4: Eu^{3+} nanosheres and mocrospheres [J]. Journal of Physical Chemistry C, 2010, 114: 14018−14024.

[28] SUN Y G, GATES B, MAYERS B, XIA Y N. Crystalline silver nanowires by soft solution processing [J]. Nano Letters, 2002, 2: 165−168.

[29] FAN Xi-mei, ZHOU Zuo-wan, WANG Jie, TIAN Ke. Morphology and optical properties of tetrapod-like zinc oxide whiskers synthesized via equilibrium gas expanding method [J]. Transactions of Nonferrous Metals Society of China, 2011, 21: 2056−2060.

[30] RODRIGUEN J A, JIRSAK T, CHATURVEDI S, KUHN M. Reaction of SO_2 with ZnO $(000\bar{1})$ -O and ZnO powders: Photoemission and XANES studies on the formation of SO_3 and SO_4 [J]. Surface Science, 1999, 442: 400−412.

[31] WAGNER C D, RIGGS W W, DAVIS L E, MOULDER J F, MUILENBERG G E. Handbook of X-ray photoelectron spectroscopy [M]. Eden Prairie: Perkin-Elmer, 1979.

[32] CHEN P, GU L, CAO X B. From single ZnO multipods to hetero structured ZnO/ZnS, ZnO/ZnSe, ZnO/Bi_2S_3 and ZnO/Cu_2S multipods: controlled synthesis and tunable optical and photoelectronchemical properties [J]. Crystal Engineering Communications, 2010, 12: 3950−3958.

[33] KAUSHIK A, KUMAR J, TIWARI M K, KHAN R, MALHOTRA B D, GUPTA V, SINGH S P. Fabrication and characterization of polyaniline-ZnO hybrid nanocomposite thin film [J]. Journal of Nanoscience and Nanotechnology, 2008, 8: 1757−1761.

[34] TIAN C G, KANG Z H, WANG E, GUO L, WANG C L, XU L, HU C G. Synthesis of dodecanethiolate-protected Cu_2S nanoparticles in a two-phase system [J]. Materials Letters, 2005, 59: 1156−1160.

[35] LI X B, WANG L L, LU X H. Preparation of silver-modified TiO_2 via microwave-assisted method and its photocatalytic activity for toluence degradation [J]. Journal of Hazard Materials, 2010, 177: 639−647.

[36] CHEN T W, ZHEG Y H, LIN J M, CHEN G N. Study on the photocatalytic degradation of methyl orange in water using Ag/ZnO as catalyst by liquid chromatography electronspray ionization ion-trap mass spectrometry [J]. Journal of American Society for Mass Spectrometry, 2008, 19: 997−1003.

[37] TAN T, LI Y, LIU Y, WANG B, SONG X M. Two-step preparation of Ag/tatrapod-like ZnO with photocatalytic activity by thermal evaporation and sputtering [J]. Materials Chemistry and Physics, 2008, 111: 305−308.

[38] YU J G, XIONG J F, CHENG B, LIU S G. Fabrication and characterization of Ag−TiO_2 multiphase nanocomposite thin films with enhanced photocatalytic activity [J]. Applied Catalysis B, 2005, 60: 211−221.

[39] TENNAKONE K, BANDARA J. Photocatalytic activity of dye-sensitized tin(IV) oxide nanocrystalline particles attached to zinc oxide particles: Long distance electron transfer via ballistic transport of electrons across nanocrystallites [J]. Applied Catalysis A, 2001, 208: 335−341.

[40] LINSEBIGLER A L, LU G Q, YATES JR J T. Photocatalysis on TiO_2 surfaces: Principles, mechanism and selected results [J]. Chemical Reviews, 1995, 95: 735−758.

[41] QI L F, YU J G, JARONIEC M. Preparation and enhanced visible-light photocatalytic H_2-production activity of CdS-sensitized Pt/TiO_2 nanosheets with exposed (001) facets [J]. Physical Chemistry Chemical Physics, 2011, 13: 8915−8923.

[42] SERPONE N, MARUTHAMUTHU P, PICHAT P, PELIZZETTI E, HIDAKA H. Exploiting the interparticle electron transfer process in the photocatalysed oxidation of phenol, 2-chlorophenol and hole pentachlorophenol: Chemical evidence for electron and hole transfer between coupled semiconductors [J]. Journal of Photochemistry and Photobiology A, 1995, 85: 247−255.

[43] WEI S Q, CHEN Y Y, MA Y Y, SHAO Z G. Fabrication of CuO/ZnO composite films with cathodic co-electrodeposition and their photocatalytic performance [J]. Journal of Molecular Catalysis A, 2010, 331: 112−116.

[44] WANG J, FAN X M, WU D Z, DAI J, LIU H, LIU H R, ZHOU Z W. Fabrication of $CuO/T\text{-}ZnO_w$ nanocomposites using photo-deposition and their photocatalytic property [J]. Applied Surface Science, 2011, 258: 1797−1805.

[45] ZHANG J, YU J G, ZHANG Y M, LI Q, GONG J R. Visible light photocatalytic H_2-production activity of CuS/ZnS porous nanosheets based on photoinduced interfacial charge teansfer [J]. Nano Letters, 2011, 11: 4774−4779.

[46] YU J G, RAN J R. Facile preparation and enhanced photocatalytic H_2-production activity of $Cu(OH)_2$ cluster modified TiO_2 [J]. Energy Environmental Science, 2011, 4: 1364−1371.

[47] RAJESHWAR K, OSUGI M E, CHANMANEE W, CHENTHAMARAKSHAN C R, ZANONI M V B, KAJITVICHYANUKUl P, KRISHNAN-AYER R. Heterogeneous photocatalytic treatment of organic dyes in air and aqueous media [J]. Journal of Photochemistry and Photobiology C, 2008, 9: 171−192.

硫化亚铜/四针状氧化锌晶须异质结的多元醇法制备及光催化性能

吴德智，范希梅，田 轲，代 佳，刘花蓉

西南交通大学 材料科学与工程学院，材料先进技术教育部重点实验室，成都 610031

摘 要：以聚乙烯吡咯烷酮(PVP)为表面活性剂，通过多元醇法制备 $Cu_2S/T\text{-}ZnO_w$ 异质结复合材料，利用 XRD、FESEM、EDS、XPS 和 FTIR 测试方法对样品进行表征，通过测定甲基橙溶液的光降解率来评价样品的光催化活性。结果表明，在紫外光照射下，$Cu_2S/T\text{-}ZnO_w$ 纳米复合材料的光催化性能优于纯氧化锌晶须的。当 PVP 的浓度为 3.0 g/L 时，样品的光催化活性最高，在紫外光照射 120 min 后，甲基橙的降解率为 97%。经过 4 个周期的光催化实验后，$Cu_2S/T\text{-}ZnO_w$ 催化剂的光催化活性并没有明显下降，说明该样品具有优异的光稳定性。此外，讨论了 $Cu_2S/T\text{-}ZnO_w$ 纳米复合材料的光催化机理。

关键词：$Cu_2S/T\text{-}ZnO_w$ 异质结；光催化性能；硫化亚铜纳米颗粒

(Edited by LI Xiang-qun)